PAPER

# Total branching ratio of the $K^-$ two-nucleon absorption in $^{12}C$

IOP Publishing Physica Scripta
Phys. Scr. **95** (2020) 084012 (6pp) https://doi.org/10.1088/1402-4896/ab9ed3

# Total branching ratio of the $K^-$ two-nucleon absorption in $^{12}C$

**R Del Grande[1,2], K Piscicchia[2,1], M Cargnelli[3], C Curceanu[2], L Fabbietti[4,5], J Marton[3], P Moskal[6], A Ramos[7], A Scordo[2], D Sirghi[2], M Skurzok[2,6], O Vazquez Doce[4,5], S Wycech[8], J Zmeskal[3], V De Leo[9,10], G Mandaglio[11,12], M Martini[2,13], E Perez Del Rio[9,10], A Selce[14,15] and M Silarski[6]**

[1] Centro Fermi—Museo Storico della Fisica e Centro Studi e Ricerche 'Enrico Fermi', 00184 Rome, Italy
[2] INFN—Laboratori Nazionali di Frascati, 00044 Frascati, Italy
[3] Stefan-Meyer-Institut für Subatomare Physik, 1090 Wien, Austria
[4] Excellence Cluster 'Origin and Structure of the Universe', 85748 Garching, Germany
[5] Physik Department E12, Technische Universität München, 85748 Garching, Germany
[6] Institute of Physics, Jagiellonian University, 30-348 Cracow, Poland
[7] Departament de Fisica Quantica i Astrofisica and Institut de Ciencies del Cosmos, Universitat de Barcelona, 08028 Barcelona, Spain
[8] National Centre for Nuclear Research, 00681 Warsaw, Poland
[9] Dipartimento di Fisica dell'Università 'Sapienza', 00185 Roma, Italy
[10] INFN Sezione di Roma, 00185 Roma, Italy
[11] Dipartimento di Scienze Matematiche e Informatiche, Scienze Fisiche e Scienze della Terra dell'Università di Messina, 98122 Messina, Italy
[12] INFN Sezione di Catania, 95123 Catania, Italy
[13] Dipartimento di Scienze e Tecnologie applicate, Università 'Guglielmo Marconi', 00193 Roma, Italy
[14] Dipartimento di Matematica e Fisica dell'Università 'Roma Tre', 00146 Roma, Italy
[15] INFN Sezione di Roma Tre, 00146 Roma, Italy

E-mail: raffaele.delgrande@lnf.infn.it

Received 9 March 2020, revised 10 June 2020
Accepted for publication 22 June 2020
Published 10 July 2020

**Abstract**

This work is a critical re-analysis of the results obtained by the AMADEUS collaboration, concerning the measurement of the $K^-$ multi-nucleon absorption reactions, on a $^{12}C$ target, in the $\Lambda p$ final state (Del Grande et al 2019 *Eur. Phys. J.* C **79**, 190). We show that a good estimate of the $K^-$ two-nucleon absorption total branching ratio can be extracted, given that the measured final state interactions and conversion reactions contain information on almost all the remaining hyperon-nucleon final state combinations. The main contribution to the total branching ratio of the $K^-$ two-nucleon absorption in Carbon is extracted from the measured ratios and is found to be $(16.1 \pm 2.9(\text{stat.})^{+4.3}_{-5.5}(\text{syst.}))\%$, which is in agreement with recent theoretical predictions. The missing contribution, from those few channels for which a $\Lambda p$ pair could not be detected in the final state of the interaction, is also estimated combining both the measured branching ratios and the available theoretical information, and amounts to $(5.5 \pm 0.1(\text{stat.})^{+1.0}_{-0.9}(\text{syst.}))\%$. All together the total branching ratio of the $K^-$ two-nucleon absorption in Carbon is found to be $(21.6 \pm 2.9(\text{stat.})^{+4.4}_{-5.6}(\text{syst.}))\%$.

Keywords: strong interaction, strangeness nuclear physics, antikaon-nucleon interaction

(Some figures may appear in colour only in the online journal)

 

## 1. Introduction

The strong interaction, described by the Quantum Chromodynamics (QCD) theory, is still not yet well understood at the low-energies frontier, in the so-called non-perturbative regime. This difficulty is connected to the non-abelian character of the strong interaction, linked to the fact that gluons are QCD-charged particles (they carry colours). For a deeper understanding of the QCD, experimental data, especially in low-energy regime, are badly needed, to fuel the models and effective QCD theories and approaches, presently under development. Among the experimental studies, those involving 'strange' particles, i.e. having a strange quark inside, play a special role, due to the fact that the strange quark mass is in between that of the lightest quarks ($u$, $d$) and the one of the heavy quarks ($c$, $b$, $t$). Such studies allow to test a broad class of models/theories, which have an impact going from particle and nuclear physics to astrophysics.

In this context the AMADEUS collaboration aims to provide experimental constraints to the low-energy interaction of antikaons, containing a strange quark, with nucleons. The antikaon-nucleon ($\bar{\mathrm{K}}$ N) interaction is the ideal testing ground to explore the fundamental symmetries of the strong interaction. In the low-energy regime the interplay between spontaneous and explicit chiral symmetry breaking emerges, as a consequence of the large strange quark mass with respect to the $u$ and $d$ quark masses [1]. Motivated by colour confinement, effective field theories are introduced, having mesons and baryons as fundamental degrees of freedom instead of quarks and gluons. Due to the existence of broad resonances (the isospin $I = 0$ $\Lambda(1405)$ and the isospin $I = 1$ $\Sigma(1385)$) in the $\bar{\mathrm{K}}$N sub-threshold region, chiral perturbation theory can not be applied. Therefore, chiral unitary approaches [2–6] or phenomenological models [7, 8] are introduced. The predicted $s$-wave $\mathrm{K^-p}$ and $\mathrm{K^-n}$ scattering amplitudes, and the positions of the corresponding poles, are strongly model dependent [9]. The $\mathrm{K^-p}$ interaction at threshold is constrained by the measured shift and width of kaonic hydrogen [10] (see also [11] for a complete review); the corresponding information in the $\mathrm{K^-n}$ channel will be extracted from the kaonic deuterium measurement [12, 13]. Experimental information above the threshold, at low kaon momenta ($p_{\mathrm{K}} < 120$ MeV/c), is strongly demanded. Below the threshold just one measurement exists, for the modulus of the $s$-wave $\mathrm{K^-n}$ scattering amplitude [14, 15].

Recent theoretical calculations also renewed the interest for the $\mathrm{K^-}$ multi-nucleon absorption reactions. In [16] it is shown that $\mathrm{K^-}$-nuclear optical potentials based on $\mathrm{K^-N}$ scattering amplitudes fail to reproduce the kaonic atoms data along the periodic table of the elements, unless a $\mathrm{K^-}$ multi-nucleon phenomenological potential term is added. In [17, 18] the $\mathrm{K^-}$ two-nucleon ($\mathrm{K^-}$2NA) interaction process was approached by means of a microscopic description of the three body problem. In [18] the Branching Ratios (BRs) were calculated for all the hyperon-nucleon final states at various baryon densities. Important experimental tests to the models can be provided by the measurement of the $\mathrm{K^-}$ two, three and four nucleon absorption (2NA, 3NA and 4NA) on different nuclear targets, i.e. at various nuclear densities [19–22].

In [19] the BRs and low-energy cross sections for the $\mathrm{K^-}$ 2NA, 3NA and 4NA were extracted for $\mathrm{K^-}$ capture on $^{12}$C nuclei giving rise to $\Lambda$p correlated production in the final state of the interaction. The detected $\Lambda$p pairs can be produced in Quasi-Free (QF) processes, either with a direct $\Lambda$ production, or as a result of the $\Sigma^0 \rightarrow \Lambda\gamma$ decay. Final State Interactions (FSIs), as well as $\Sigma\mathrm{N} \rightarrow \Lambda\mathrm{N}'$ conversion processes, can also occur and are found to give a dominant contribution to the $\Lambda$p final state (in agreement with the result in [23]). As described in this paper a comprehensive description of all the contributions listed above, to the measured $\Lambda$p distributions, allows to extract an estimate of the total BR of the $\mathrm{K^-}$ 2NA in Carbon. The BRs of those few final states outside the acceptance of the measurements in [19] are carefully estimated and presented in section 3.

The paper is organised as follows: in section 2 the results obtained in [19] are summarised; the details of the FSI and conversion processes simulations are given in section 3, where a total 2NA BR is extracted and the few missing contributions are estimated; the conclusions are given in the section 4.

## 2. Details of the data analysis

The AMADEUS collaboration is analysing the data collected with the KLOE detector during the 2004/2005 data taking campaign, corresponding to 1.74 fb$^{-1}$ total integrated luminosity. Low-momentum and monochromatic $\mathrm{K^-}$s ($p_{\mathrm{K}} \sim 127$ MeV/c), produced at the DA$\Phi$NE collider [24] from the $\phi$-meson decay nearly at-rest, are absorbed in the materials of the KLOE detector [25] used as an active target. The $\mathrm{K^-}$ absorptions at-rest and in-flight in the nuclei contained in the beam pipe and detector materials (H, $^4$He, $^9$Be and $^{12}$C) are investigated reconstructing the emitted hyperon-pion (Y$\pi$) [15] and hyperon-nucleon/nuclei (YN/multi-N) pairs [19, 21, 22] in the final state. In [19] a pure sample of $\Lambda$p correlated production events was reconstructed, when the $\mathrm{K^-}$ is absorbed in the entrance wall of the KLOE drift chamber, which is an almost pure Carbon target. The events selection was optimised in order to reject the pionic processes, the production of a hyperon-pion pair being the signature of a $\mathrm{K^-}$ single-nucleon absorption. When a $\mathrm{K^-}$ absorption occurs on a single nucleon, protons in the final state of the interaction originate only in nuclear fragmentations. Such protons are characterised by a Fermi momentum distribution. The key selection criterion is then represented by the measurement of the protons mass by Time Of Flight (TOF). For the measurement of the mass, information on the time and on the protons energy from the calorimeter is needed. The calorimeter momentum threshold ($p_{\mathrm{p}} > 240$ MeV/c) efficiently discards the majority of the 'Fermi' protons from nuclear fragmentations. A pure sample of $\mathrm{K^-}$ multi-nucleon absorption processes was then selected. The detected $\Lambda$s can be produced (i) directly in the $\mathrm{K^-}$

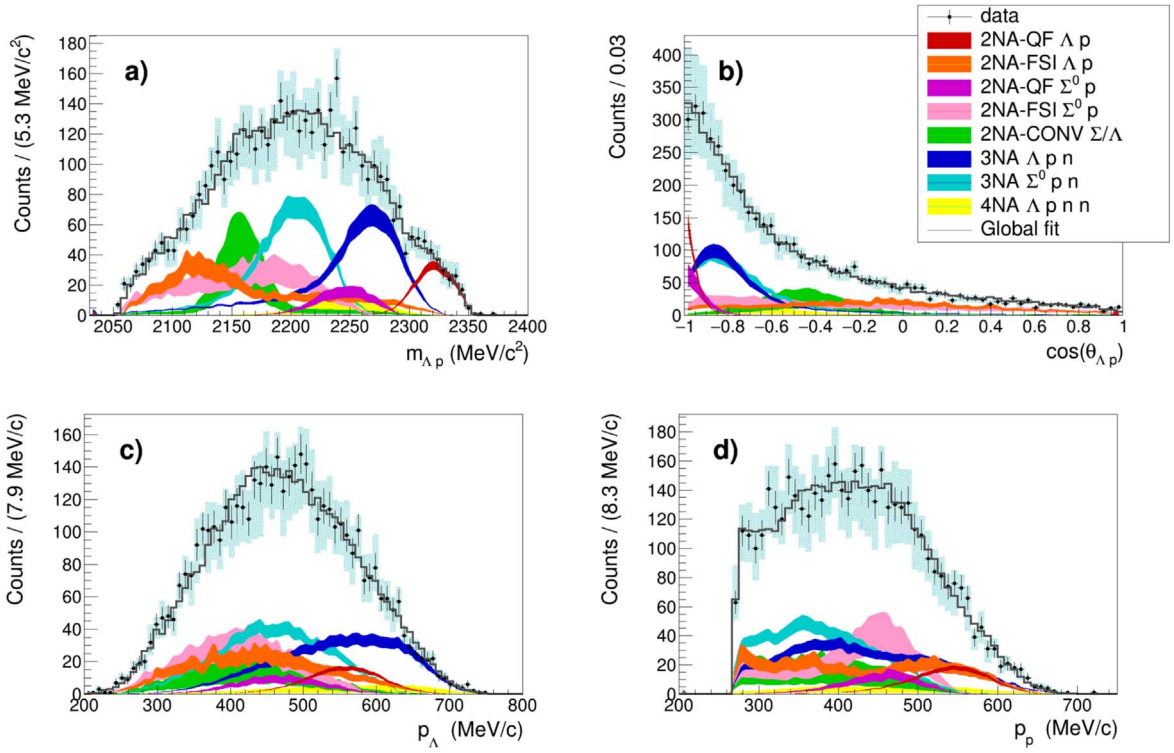


**Figure 1.** Λp invariant mass (panel a), Λp angular correlation (panel b), Λ momentum (panel c) and proton momentum (panel d) distributions are shown for the $K^-$ absorption on $^{12}C$ listed in the legend. Black points represent the data, black error bars correspond to the statistical errors, cyan error bars correspond to the systematic errors. The grey line distributions represent the global fitting functions, the coloured distributions represent the contributing processes according to the colour code reported in the legend and the widths correspond to the statistical error. The figure is adapted from [19] with kind permission of The European Physical Journal (EPJ).

multi-nucleon absorption (ii) as secondary products of a $\Sigma^0$ decay ($\Sigma^0 \rightarrow \Lambda\gamma$) or a $\Sigma$ conversion ($\Sigma N \rightarrow \Lambda N'$).

Monte Carlo (MC) simulations of the $K^-$ 2NA, 3NA and 4NA were performed based on [14, 26] for both at-rest and in-flight $K^-$ captures in $^{12}C$ nuclei. In the case of the $K^-$ 2NA, three contributions were considered: (1) the QF production of the $\Lambda(\Sigma^0)$p pairs, i.e. without FSIs with the residual nucleons; (2) the primary $\Lambda(\Sigma^0)$N production followed by elastic FSIs (only single collisions of the hyperon or the nucleon with the residual nucleus are accounted for); (3) the primary $\Sigma$N production followed by the inelastic $\Sigma N \rightarrow \Lambda N'$ conversion reaction. Further details of the simulations for the processes (2) and (3) are given in section 3.

A simultaneous $\chi^2$ fit of the measured Λp invariant mass ($m_{\Lambda p}$), Λp angular correlation ($\cos\theta_{\Lambda p}$), Λ momentum ($p_\Lambda$) and proton momentum ($p_p$) was performed. The result of the fit is shown in figure 1. The reduced chi-squared is $\chi^2/dof = 194/206 = 0.94$.

From the fit the BRs (for the at-rest $K^-$ captures) and the cross sections (for the in-flight $K^-$ captures) of all the processes contributing to the measured Λp events are extracted and summarised in table 1.

## 3. Measurement of the total 2NA branching ratio

Starting from the BRs listed in table 1 we give an estimate of the total $K^-$ 2NA BR for captures on $^{12}C$; a few channels are missing in this estimate, for which we can not detect a Λp pair in the final state. The missing contribution from these channels is evaluated taking advantages of the theoretical and experimental results obtained in [18, 27].

The $K^-$ 2NA-FSI and the conversion processes, used to fit the measured Λp distributions, were simulated as two steps reactions. The primary interaction is

$$K^- + {}^{12}C \rightarrow K^- + \text{'NN'} + R \rightarrow Y + N + R \qquad (1)$$

where 'NN' are the absorbing nucleons bound in the Carbon nucleus, R represents the residual nucleus ($^{10}$Be or $^{10}$B), Y and N are the produced hyperon and nucleon. Two types of FSIs can give rise to the measured Λp final state (the particular case of the hyperon conversion is treated separately for the sake of clarity): (i) the detected proton corresponds to the proton produced in the primary interaction (with or without having suffered re-scattering on the residual) (ii) the detected proton is a fragment of R produced in the re-scattering. The primary pairs contributing to the observed Λp final state are Λp, Λn, $\Sigma^0$p, $\Sigma^0$n; the secondary interaction can then be schematically represented as:

$$Y + R \rightarrow Y + \text{'N'} + R' \rightarrow Y + N' + R' \qquad (2)$$

or

$$N + R \rightarrow N + \text{'N'} + R' \rightarrow N + N' + R' \qquad (3)$$

being N′ and R′ the nucleon and the residual emerging in the FSI process. The calculated Λp invariant mass distributions for the $K^-$ 2NA processes producing a primary ΛN pair,

**Table 1.** Branching ratios (for the $K^-$ absorbed at-rest) and cross sections (for the $K^-$ absorbed in-flight) of the $K^-$ multi-nucleon absorption processes. The $K^-$ momentum is evaluated in the centre of mass reference frame of the absorbing nucleons, thus it differs for the 2NA and 3NA processes. The statistical and systematic errors are also given. The table is adapted from [19] with kind permission of The EPJ.

| Process | Branching Ratio (%) | $\sigma$ (mb) | @ $p_K$ (MeV/c) |
|---|---|---|---|
| 2NA-QF $\Lambda$p | $0.25 \pm 0.02$ (stat.) $^{+0.01}_{-0.02}$(syst.) | $2.8 \pm 0.3$ (stat.) $^{+0.1}_{-0.2}$ (syst.) | @ $128 \pm 29$ |
| 2NA-FSI $\Lambda$p | $6.2 \pm 1.4$(stat.) $^{+0.5}_{-0.6}$(syst.) | $69 \pm 15$ (stat.) $\pm 6$ (syst.) | @ $128 \pm 29$ |
| 2NA-QF $\Sigma^0$p | $0.35 \pm 0.09$(stat.) $^{+0.13}_{-0.06}$(syst.) | $3.9 \pm 1.0$ (stat.) $^{+1.4}_{-0.7}$ (syst.) | @ $128 \pm 29$ |
| 2NA-FSI $\Sigma^0$p | $7.2 \pm 2.2$(stat.) $^{+4.2}_{-5.4}$(syst.) | $80 \pm 25$ (stat.) $^{+46}_{-60}$ (syst.) | @ $128 \pm 29$ |
| 2NA-CONV $\Sigma$ /$\Lambda$ | $2.1 \pm 1.2$(stat.) $^{+0.9}_{-0.5}$(syst.) | — | |
| 3NA $\Lambda$p–n | $1.4 \pm 0.2$(stat.) $^{+0.1}_{-0.2}$(syst.) | $15 \pm 2$ (stat.) $\pm 2$ (syst.) | @ $117 \pm 23$ |
| 3NA $\Sigma^0$ p–n | $3.7 \pm 0.4$(stat.) $^{+0.2}_{-0.4}$(syst.) | $41 \pm 4$ (stat.) $^{+2}_{-5}$ (syst.) | @ $117 \pm 23$ |
| 4NA $\Lambda$pnn | $0.13 \pm 0.09$(stat.) $^{+0.08}_{-0.07}$(syst.) | — | |
| Global $\Lambda(\Sigma^0)$p | $21 \pm 3$(stat.) $^{+5}_{-6}$(syst.) | - | |

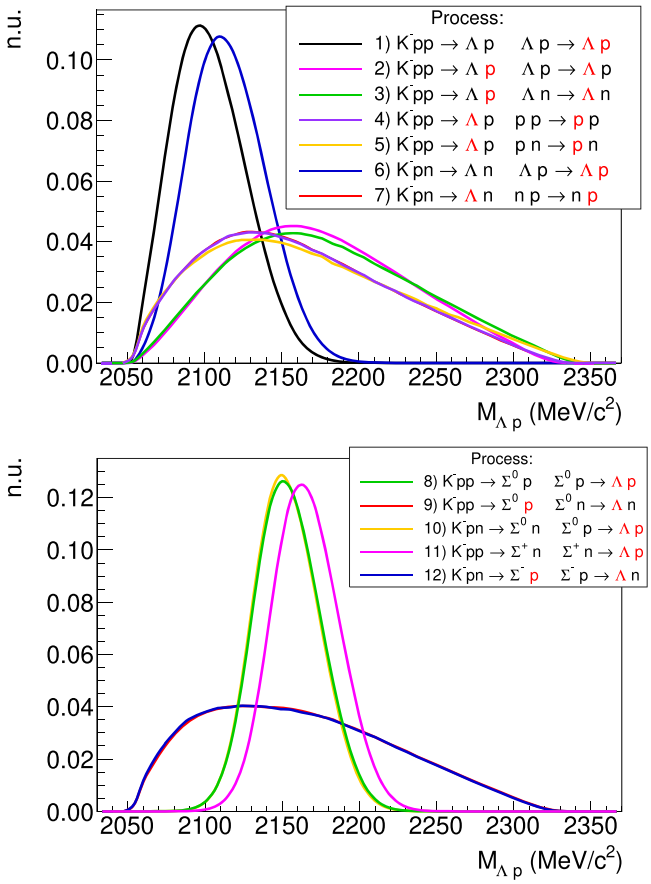


**Figure 2.** Calculated invariant mass distributions for the $\Lambda$p pairs produced in FSI (top panel) and in the $\Sigma/\Lambda$ conversion processes (bottom panel). The legend shows the considered elementary reactions: the primary productions according to equation (1) in the text (left column) and the secondary interactions as given by equations (2)–(3) in the text (right column). The distributions refer to the $\Lambda$p pairs marked in bold red.

followed by FSI and contributing to the measured $\Lambda$p sample are shown in figure 2 top panel. Left column of the legend corresponds to the primary interaction equation (1). Right column of the legend corresponds to the secondary interaction equations (2)–(3). The detected particles (from which the invariant mass is built) are marked with bold red colour. The processes (1, 6), (2, 3) and the reactions (4, 5, 7) are characterised by similar shapes in all the relevant kinematic distributions; hence, they are not experimentally distinguishable given the available resolutions. For these groups of similar reactions one shape is considered in the fit for each kinematic variable, corresponding to a free parameter. All the other processes contribute to the fit independently. The orange distribution in figure 1 is the weighted sum of all the independent reactions, the weights corresponding to the parameters which minimise the $\chi^2$ function.

An analogous procedure is applied when a $\Sigma^0$ or a charged $\Sigma$ is produced with a nucleon in the primary interaction, followed by the conversion:

$$\Sigma + \mathrm{R} \rightarrow \Sigma + \text{`N'} + \mathrm{R}' \rightarrow \Lambda + \mathrm{N}' + \mathrm{R}'. \qquad (4)$$

The corresponding invariant mass distributions are shown in figure 2 bottom panel.

From the discussion above it emerges that the sum of all the BRs for the $K^-$ 2NA reactions (with or without FSIs or conversion) amounts with good approximation to the total BR of the $K^-$ 2NA; more precisely it corresponds to the total $K^-$ 2NA BR with the following missing contributions:

- the $\Sigma^-$n primary production, which could give rise to the observed $\Lambda$p in the final state of the interaction as a result of a double collision (both of the $\Sigma^-$ and the neutron in the secondary interaction step). Such a reaction was not accounted for in the analysis. The BR of this process is quoted in [18] to be $(0.12 \pm 0.01(\text{syst.}))\%$. The uncertainty on the BR is due to the systematic effect introduced by the cut-off on the $K^-$NN potential which is applied in the calculation [18];
- the QF $\Lambda$n and $\Sigma^0$n productions. The contributions of these reactions can be easily obtained. Given that for a nucleon momentum of the order of 560 MeV/c (typical momentum of the primarily produced nucleons) the n-n and p–n scattering cross sections are comparable, we can assume that the ratio of the QF [19] over the total

production [18]

$$P_{QF}^{YN} = \frac{BR_{QF}(YN)}{BR(YN)}, \quad (5)$$

is the same for the $\Lambda n$ ($\Sigma^0 n$) and $\Lambda p$ ($\Sigma^0 p$) channels. Using this ratio and the total $\Lambda n$ and $\Sigma^0 n$ production BRs [18] the BR of the QF $\Lambda n$ and $\Sigma^0 n$ productions is found to be

$$\begin{aligned} &BR_{QF}(\Lambda n) + BR_{QF}(\Sigma^0 n) \\ &= BR(\Lambda n) \cdot P_{QF}^{\Lambda p} + BR(\Sigma^0 n) \cdot P_{QF}^{\Sigma^0 p} \\ &= (0.76 \pm 0.09(\text{stat.})^{+0.13}_{-0.06}(\text{syst.}))\%. \end{aligned} \quad (6)$$

The statistical error is obtained propagating the corresponding uncertainties of the measured BRs (table 1). The systematic errors originate from propagation of the systematic uncertainties on the experimental BRs (table 1) and the systematics which are involved in the theoretical calculation [18];

- the FSI of primarily produced $\Lambda n$ and $\Sigma^0 n$ pairs without the emission of a proton in the re-scattering on the residual nucleons. The probability of the YN pairs to perform FSI with the residual nucleus can be estimated as:

$$P_{FSI}^{YN} = 1 - P_{QF}^{YN} = 1 - \frac{BR_{QF}(YN)}{BR(YN)}. \quad (7)$$

In the case of primary $\Sigma^0 n$ production the secondary processes in equations (2)–(3)–(4) contribute to the probability in equation (7) as follows

$$\begin{aligned} P_{FSI}^{\Sigma^0 n} = &P(\Sigma^0 p \to \Sigma^0 p) + P(\Sigma^0 n \to \Sigma^0 n) \\ &+ P(\Sigma^0 p \to \Lambda p) + P(\Sigma^0 n \to \Lambda n) \\ &+ P(np \to np) + P(nn \to nn). \end{aligned} \quad (8)$$

Given that the residual Boron-10 has equal amount of neutrons and protons and assuming isospin symmetry we have $P(\Sigma^0 p \to \Sigma^0 p) = P(\Sigma^0 n \to \Sigma^0 n)$, $P(\Sigma^0 p \to \Lambda p) = P(\Sigma^0 n \to \Lambda n)$ and $P(np \to np) = P(nn \to nn)$. The probability that $\Sigma^0$ or neutron undergo FSI without producing a proton in the final state is:

$$P(\Sigma^0 n \to \Sigma^0 n) + P(\Sigma^0 n \to \Lambda n) + P(nn \to nn) = \frac{1}{2} P_{FSI}^{\Sigma^0 n}. \quad (9)$$

The corresponding BR is

$$BR_{miss}(\Sigma^0 n) = BR(\Sigma^0 n)\frac{1}{2} P_{FSI}^{\Sigma^0 n} = BR(\Sigma^0 n)\frac{1}{2}(1 - P_{QF}^{\Sigma^0 n}), \quad (10)$$

where the $BR(\Sigma^0 n)$ is given in [18] and $P_{QF}^{YN}$ is obtained combining the theoretical calculations [18] and the measured BRs in table 1. In the case of primary $\Lambda n$ production, following the same procedure, we find

$$BR_{miss}(\Lambda n) = BR(\Lambda n)\frac{1}{2} P_{FSI}^{\Lambda n} = BR(\Lambda n)\frac{1}{2}(1 - P_{QF}^{\Lambda n}). \quad (11)$$

The missing contribution is then given by:

$$\begin{aligned} &BR_{miss}(\Sigma^0 n) + BR_{miss}(\Lambda n) \\ &= (1.62 \pm 0.04(\text{stat.})^{+0.22}_{-0.21}(\text{syst.}))\%. \end{aligned} \quad (12)$$

The statistical error is obtained propagating the corresponding uncertainties of the measured BRs (table 1). The systematic errors are derived by propagating the systematic uncertainties on the experimental BRs (table 1) and the systematics which are involved in the theoretical calculation [18]. It is worth to notice that, whether the primary produced Y or neutron re-scatter with a neutron, a proton in the final state is always produced because a Boron-9 is left as a residual of the FSI which is unstable with respect to the proton emission reaction: $^9B \to p + 2^4He$ (the mean lifetime is of about $10^{-20}$s [28]). By a dedicated simulation we estimate the maximum momentum achieved by these protons to be less than about 130 MeV/c. The experimental detection efficiency for such low momentum protons is negligible due to the mass requirement by TOF;

- the contribution due to the $\Sigma^+$ and $\Sigma^-$ hyperons which do not convert into a $\Lambda$ hyperon. It is not trivial to estimate this contribution because all the conversion probabilities quoted in literature refer to the conversion of charged $\Sigma$s which are produced in $K^-$ single nucleon absorptions. We then take as a reference value a conversion probability (for both $\Sigma^+$ and $\Sigma^-$ particles) of $C_\Sigma = 0.62 \pm 0.02(\text{syst.}) \pm 0.04(\text{syst.})$ (see [27]). As a consequence, the BR of the missing contribution is found to be

$$\begin{aligned} BR_{no-conv} &= BR(\Sigma^- p)(1 - C_{\Sigma^-}) + BR(\Sigma^+ n)(1 - C_{\Sigma^+}) \\ &= (3.04 \pm 0.03(\text{stat.}) \pm 0.92(\text{syst.}))\%. \end{aligned} \quad (13)$$

The branching ratios $BR(\Sigma^- p)$ and $BR(\Sigma^+ n)$ are taken from [18]. The statistical error is calculated propagating the corresponding uncertainties of the measured conversion probabilities [27]. The systematic error is obtained from propagation of the systematic uncertainties on the experimental conversion probability [27] and the systematics which are involved in the theoretical calculation [18].

Summarizing, the global $K^-$ 2NA BR for all those processes in $^{12}C$ which give rise to the production of a $\Lambda p$ pair in the final state of the interaction (both in direct production, or following any kind of FSI or conversion) is measured to be:

$$\begin{aligned} &BR_{\Lambda p \text{ final state}}(K^- 2NA \to YN) \\ &= (16.1 \pm 2.9(\text{stat.})^{+4.3}_{-5.5}(\text{syst.}))\%, \end{aligned} \quad (14)$$

obtained as the sum of the measured BRs of all the $K^-$ 2NA contributions listed in table 1. This is an estimate of the total $K^-$ 2NA BR, but misses those few processes without a $\Lambda p$ in the final state. Still, a good estimate of the missing contribution can be given combining the measured BRs in table 1 with the available theoretical/experimental information in literature, and results to be:

$$BR_{missing} = (5.5 \pm 0.1(\text{stat.})^{+1.0}_{-0.9}(\text{syst.}))\%. \quad (15)$$

Finally we can infer the total BR of the $K^-$ 2NA in Carbon, which is the sum of equations (14) and (15):

$$\mathrm{BR}(K^-2NA \rightarrow YN) = (21.6 \pm 2.9(\mathrm{stat.})^{+4.4}_{-5.6}(\mathrm{syst.}))\%. \quad (16)$$

## 4. Conclusions

In this work the total $K^-$ 2NA BR in $^{12}C$ is estimated based on the measurement of the corresponding ratios having a $\Lambda p$ in the final state given in [19]. This is made possible by the fact that final state interactions and $\Sigma/\Lambda$ conversion processes (carefully quantified in [19]) dominate in the observed $\Lambda p$ final state, thus containing rich information on almost all the remaining hyperon-nucleon final state combinations.

The main contribution to the total BR of the $K^-$ 2NA in Carbon, obtained by summing the BRs measured in [19], is found to be $(16.1 \pm 2.9(\mathrm{stat.})^{+4.3}_{-5.5}(\mathrm{syst.}))\%$, in agreement with the recent prediction in [18] at 0.3 $\rho_0$ baryon density, which is the relevant density region for the absorption of low-energy $K^-$ on $^{12}C$ nuclei. The missing contribution from those few channels for which a $\Lambda p$ pair can not be detected in the final state of the interaction is also estimated and amounts to $(5.5 \pm 0.1(\mathrm{stat.})^{+1.0}_{-0.9}(\mathrm{syst.}))\%$. Including the missing component, the total BR of the $K^-$ 2NA in Carbon is found to be $(21.6 \pm 2.9(\mathrm{stat.})^{+4.4}_{-5.6}(\mathrm{syst.}))\%$.

## Acknowledgments

We acknowledge the KLOE/KLOE-2 Collaboration for their support and for having provided us with the data and the tools to perform the analysis presented in this paper. Part of this work was supported by Minstero degli Affari Esteri e della Cooperazione Internazionale, Direzione Generale per la Promozione del Sistema Paese (MAECI), Strange Matter project PRG00892; EU STRONG-2020 project (grant agreement No 824 093); Polish National Science Center through grant No. UMO-2016/21/D/ST2/01155.

## ORCID iDs

R Del Grande https://orcid.org/0000-0002-7599-2716

## References

[1] Weise W 2015 Topics in low-energy QCD with strange quarks *Hyperfine Interact.* **233** 131–40
[2] Ikeda Y, Hyodo T and Weise W 2012 Chiral SU(3) theory of antikaon-nucleon interactions with improved threshold constraints *Nucl. Phys.* A **881** 98–114
[3] Cieply A and Smejkal J 2012 Chirally motivated $\bar{K}N$ amplitudes for in-medium applications *Nucl. Phys.* A **881** 115–26
[4] Guo Z-H and Oller J A 2013 Meson-baryon reactions with strangeness -1 within a chiral framework *Phys. Rev.* C **87** 035202
[5] Mai M and Meißner U-G 2015 Constraints on the chiral unitary $\bar{K}N$ amplitude from $\pi\Sigma K^+$ photoproduction data *Eur. Phys. J.* A **51** 30
[6] Feijoo A, Magas V and Ramos A 2019 $S = -1$ meson-baryon interaction and the role of isospin filtering processes *Phys. Rev.* C **99** 035211
[7] Akaishi Y and Yamazaki T 2002 Nuclear anti-K bound states in light nuclei *Phys. Rev.* C **65** 044005
[8] Staronski L R and Wycech S 1987 Nuclear absorption of $K^-$ and models of $\Lambda(1405)$ *J. Phys. G: Nucl. Phys.* **13** 1361–73
[9] Cieplý A, Mai M, Meißner U-G and Smejkal J 2016 On the pole content of coupled channels chiral approaches used for the $\bar{K}N$ system *Nucl. Phys.* A **954** 17–40
[10] Bazzi M *et al* 2011 A new measurement of kaonic hydrogen x-rays *Phys. Lett.* B **704** 113
[11] Curceanu C *et al* 2019 The modern era of light kaonic atom experiments *Rev. Mod. Phys.* **91** 025006
[12] Curceanu C *et al* 2020 Kaonic Deuterium Measurement with SIDDHARTA-2 on DAΦNE *Acta Phys. Polon.* B **51** 251
[13] Bazzi M *et al* 2013 Preliminary study of kaonic deuterium x-rays by the siddharta experiment at dane *Nucl. Phys.* A **907** 77
[14] Piscicchia K, Wycech S and Curceanu C 2016 On the $K^-{}^4He \rightarrow \Lambda\pi^-{}^3He$ resonant and non-resonant processes *Nucl. Phys.* A **954** 75–93
[15] Piscicchia K *et al* 2018 First measurement of the $K^-n \rightarrow \Lambda\pi^-$ non-resonant transition amplitude below threshold *Phys. Lett.* B **782** 339–45
[16] Friedman E and Gal A 2017 $K^-N$ amplitudes below threshold constrained by multinucleon absorption *Nucl. Phys.* A **959** 66–82
[17] Sekihara T, Jido D and Kanada-En'yo Y 2009 Lambda(1405)-induced non-mesonic decay in kaonic nuclei *Phys. Rev.* C **79** 062201
[18] Hrtánková J and Ramos A 2020 Single- and two-nucleon antikaon absorption in nuclear matter with chiral meson-baryon interactions *Phys. Rev.* C **101** 035204
[19] Del Grande R *et al* 2019 $K^-$ multi-nucleon absorption cross sections and branching ratios in $\Lambda p$ and $\Sigma^0 p$ final states *Eur. Phys. J.* C **79** 190
[20] Agnello M *et al* 2015 $\Sigma^- p$ emission rates in $K^-$ absorptions at rest on $^6Li$, $^7Li$, $^9Be$, $^{13}C$ and $^{16}O$ *Phys. Rev.* C **92** 045204
[21] Vázquez Doce O *et al* 2016 $K^-$ absorption on two nucleons and $ppK^-$ bound state search in the $\Sigma^0 p$ final state *Phys. Lett.* B **758** 134–9
[22] Piscicchia K *et al* 2017 Investigation of the low-energy kaons hadronic interactions in light nuclei by amadeus *EPJ Web Conf.* **137** 09005
[23] Magas V K, Oset E, Ramos A and Toki H 2006 A Critical view on the deeply bound $K^-pp$ system *Phys. Rev.* C **74** 025206
[24] Gallo A *et al* 2006 DAFNE status report *10th European Particle Accelerator Conference (EPAC 06)* 060626 ( C) 604–6 (https://s3.cern.ch/inspire-prod-files-e/ef47f25f7b33af36f669ef96aff0da8a)
[25] Bossi F *et al* KLOE Collaboration 2008 Precision Kaon and Hadron Physics with KLOE *Riv. Nuovo Cim.* **31** 531–623
[26] Del Grande R, Piscicchia K and Wycech S 2017 Formation of $\Sigma\pi$Pairs in Nuclear Captures of $K^-$ Mesons *Acta Phys. Polon.* B **48** 1881
[27] Vander Velde-Wilquet C *et al* 1977 Determination of the branching fractions for $K^-$-meson absorptions at rest in carbon nuclei *Il Nuovo Cimento A (1965–1970)* **39** 538–47
[28] Audi G *et al* 2017 The nubase2016 evaluation of nuclear properties *Chin. Phys.* C **41** 030001